Shahrood University of Technology

Iranian Society of Mining Engineering (IRSME)

Journal of Mining and Environment (JME)

journal homepage: www.jme.shahroodut.ac.ir

THOMSON REUTERS

Evaluation of Fractal Variance-Distance Model in Identifying Geochemical Anomalies of Calamine Mehdiabad Mining Complex, Central Iran

Nasrin Sadrmohammadi[1*], Seyed Reza Mehrnia[2], Khalil Rezaei[1], Selma Kadioğlu[3], and Mahmood Honarvar[4]

1. Department of Geology, Faculty of Earth Sciences, Kharazmi University, Tehran, Iran
2. Department of Geology, Faculty of Sciences, Payam Noor University (PNU), Tehran, Iran
3. Department of Geophysical Engineering, Faculty of Engineering, Ankara University, Ankara, Turkey
4. Zap consulting engineers, Tehran, Iran

Abstract

In this paper, a power-law relation modeling called the vario-fractal model is introduced in order to understand the discrepancies between the linear and non-linear distribution of the elements and its application for mineral exploration in the calamine Zn-Pb ore-deposit. From a hypothetical viewpoint, since geochemical zonation of the supra- and sub-ore elements is a crucial evaluation criterion for concealed/underlying mineralization potentials, this hypothesis can be tested by delineating the fractal surfaces of elements as the geometric evidence of primary geochemical zonation of elements in the calamine mine. A comparison of the linear regression results with the Poisson distribution coefficients indicate the relative tendency of the elements towards a non-linear distribution. Therefore, a logarithmic equation derived from the variance-distance relationship (power-law) is used here for the delineation of fractal surfaces of elements as the geometric features related to proper self-organized distributions. In this research work, the vario-fractal expression of geochemical zonation has trace-element tendencies to the non-linear distribution. The results obtained show that the calamine's fractional surfaces are mostly of self-organized types, situated at $2 < FD < 3$ as "real fractal surfaces", although 3 of the elements appear in the quasi-fractal populations called "near Brownies" here. Moreover, the calamine's fractal surfaces can be extended throughout the anomalous regions or may be distributed as limited types of the finalized model, which is a fractal-based pattern of geochemical zonation of the elements for evaluation of the hypogenic mineralization potential and has been prioritized to 6 target-areas containing 10 elements with real fractal surfaces and 3 more at near Brownies and then validated by the mineralogical evidence.

1. Introduction

Since 1930, the non-sulfide Zn deposits, composing 11% of the total identified Zinc mines throughout the world, have been the major source of supply for the industrial and economic demands [1]. These deposits are usually hosted in dolomites and limestones within various stages of supergene mineralization. A long-term oxidation of sulfide deposits results in weathering the primary ore minerals (such as Zincite) on erosion shearing surfaces, during which hemimorphite gets concentrated in particular horizons [2, 3]. Sedimentary-hosted exhalative deposits (SEDEX)

are of a volcanogenic type, originated from deep geochemical environments and then epigenetically enriched in submarine basins. In these deposits, non-sulfide mineralization is related to post-volcanic activities occurring after a deep weathering process in surface media. Considering the condition of SEDEX ore-deposits, in which a sequence of sedimentary formations (dolomites and limestones) are in chemical reactions with volcanic solutions, a well-developed and orderly zonation of elements can be used as the geochemical keys for mineral explorations [4].

✉ *Corresponding author: nasrin_sadrmohammady@yahoo.com (N. Sadrmohammadi).*

Hence, most primary geochemical zonations of elements (PGZE) are of scale-invariant types, and power-law relations are required in order to illustrate their recursive patterns on fractal surfaces. In addition, the statistical coefficient analysis is necessary to assess the inter-relations of these elements. In the cases where deep weathering processes result in redistribution of elements (usually on eroded surfaces), geochemical disordering is the most crucial challenge to predict deep mineralization using its zonation properties, and in which cases, application of linear regression coefficients is not recommended [5, 6].

Fractal methods use the scale-invariant power-law functions to analyze the geochemical data, especially in the field of geological exploration [7-10]. A set of fractal equations mostly used for geological investigations are included as follow: concentration-area equation [11-17], spectrum-area equation [18, 19], concentration-distance equation [20], concentration-number equation [21, 22], concentration-volume equation [23, 24], and number-size equation [5, 7, 25]. Although these equations are applicable for geological studies, geochemical anomalies can be separated well by 2 or 3 of the commonly used equations. One of them is the power-law relationship between the statistical and geometrical variables used by Mark and Aronson (1984) [26] for geomorphological investigations and by Thorarinsson and Magnusson (1990) [27] for determination of Bouguer anomalies in geophysical exploration. The application of this equation has recently been proposed by Mehrnia *et al*. (2013) [28] for the non-linear estimation of Bouguer anomalies in Charak oilfield in Iran. Based on the mentioned references, the Variance-Distance (V-D) equation was used for scrutiny lithogeochemical data of the calamine Mehdiabad mine. The calamine ore-deposit that is located in the northern part of the Mehdiabad Mining Complex represents hemimorphite mineralization at the level of erosion shearing of geochemical anomalies [29]. In this non-sulfide Zn-Pb deposit, a long-time volcanic exhalation has created multiple zonations of elements in accordance with their non-linear distribution. An applicable approach, proposed here for the assessment of pathfinder elements as well as for their relations, is based on assuming the primary zonation of elements during an ore-deposit formation. It is believed that using the V-D equation helps distinguish an orderly distribution of the elements from those that are redistributed or randomly dispersed on erosion surfaces and the prognosis of concealed mineralization potential based on the calamine's geochemical distributions. Considering this, most trace-elements have a Poisson distribution (non-linear), and tend to be distributed in self-organized populations [30]. A hypogenic distribution of the elements has non-linear characteristics, in which the diversity of anomalous populations depends on the numbers and values of fractal dimensions (FDs) [31-34]. Therefore, the hypogenic distribution of the elements such as those existing in hydrothermal/volcanogenic deposits (VMS, SEDEX, etc.) can be zoned during migration of trace elements. In such cases, the delineation of self-organized populations is possible at FD =2 on the Brownian surfaces (BSs) [7]. In practice, achieving BSs (on contoured maps) and comparing their FDs with each other is a new geometric method, introduced here, in order to understand the inter-relations of elements with respect to their geochemical zonation.

2. Geographical location and geology of calamine deposit

The Mehdiabad mining complex is located 110 Km off southeast of the city of Yazd and 18 Km northeast of the Mehdiabad village. With an area of 54 hectares, the Mehdiabad calamine mine is located in the northern part of the Mehdiabad zinc-lead and barite mine (Figure 1). The calamine in this part of the mine exclusively consists of non-sulfide lead-zinc, separated from other parts by the faults. According to the geological map, scale 1:1000, the calamine stratigraphic rock units consist of sedimentary formations from the lower Cretaceous, mineralization lenses and the quaternary sediments. The host rock of calamine mine for the Abkuh formation is from the Cretaceous (Albian) period. This formation contains 4 separable units in the studied area (Figure 2). The units are Unit K_a^{sh1} (this unit is the oldest lithologic consisting of shaly lime and chert-bearing dolomitic limestone), Unit K_a^{l2} (this rock unit, as the main unit of Abkuh formation, has calamine mineralization and consists of limestone and dolomitic lime), Unit K_a^{l3} (this unit consists of a thin dark grey layer of limestone and dolomitic lime), and Unit K_a^{l4} (this inter-bed rock unit is of K_a^{l3} unit type that is composed of thick-bedded and massive cream and light grey limestone and dolomitic lime. Due to its mixture with iron oxide and hydroxide, this unit outcrops on the surface as a pinkish grey material on a relatively large syncline (lens 3) with a thickness of about 30-40 m (Figure 3)) (Figure 4).

Multiple small and large folds, and numerous fractures and faults have been created in the geological formation of the area under investigation due to various tectonic phases. The formation of the main folds of the area in a NW-SE trend indicates an effective compressional regime in the region (Figure 4). Most of the faults in the area offal into the strike-slip category [35]. The studies have revealed an interlayer relationship between the main lenses of mineralization in the calamine region and the folds of the area. In other words, the buckling resulting from the folds has created a suitable and low-pressure space for the penetration of mineralizing fluids and depositing of mineral elements. The Black-Hill fault, as one of the main faults of the area (Figure 1) has had a controlling and blocking role in the movement of the mineralizing fluids due to the less significant amount of the mineral element in the western block of this fault and a decrease in the grade of the element towards the eastern and northwestern parts. Based on the evidence of mineralization in this region, the mineralization process in this ore deposit has a close similarity to that in the MVT ore deposit.
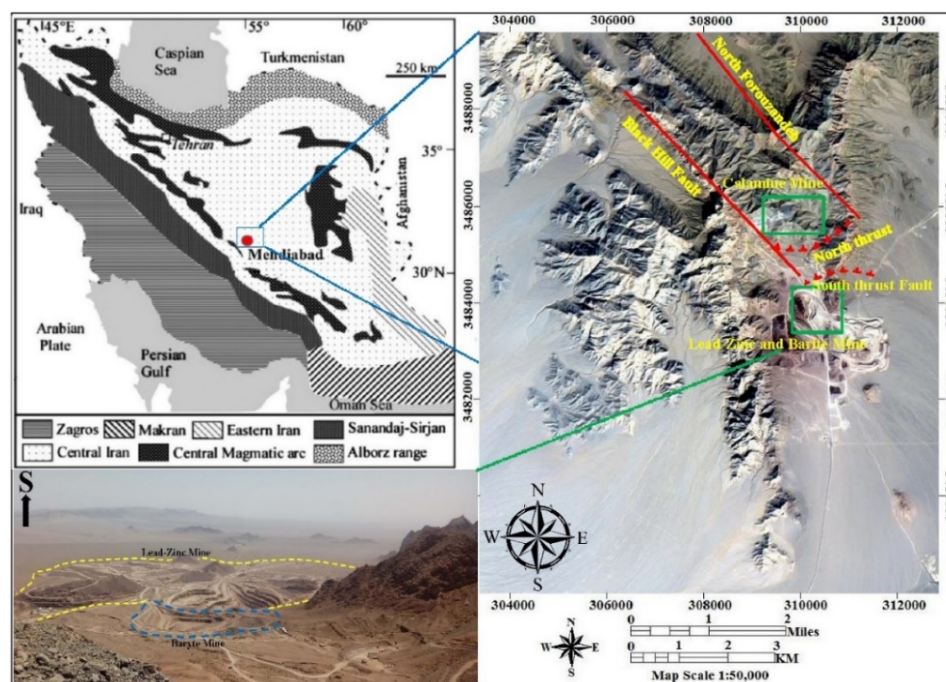

Figure 1. Location of the Mehdiabad mining complex at the southern block of Yazd and location of lead-zinc and barite mines and calamine mine between the two northern Forouzandeh and Black-Hill faults.

The mineralization outcrops in the studied area include 3 main lenses with a NNW-SSE trend and small veins and lenses [36-42] (Figure 5). Mineralization in the area include minerals of zinc (Hydrozincite, Hemimorphite, and Smithsonite) and lead (Sericite, Anglesite) oxidant zone. The Zincite and Goethite minerals have been spotted at some points (Figure 6). Other minerals including Mimetite, Hetaerolite, and Sauconite exist in small amounts. The Hemimorphite mineralization often occurs during three varied generative steps along with two monomineralic types. In some parts, calamine contains sulfide minerals of zinc and lead (Sphalerite and Galena) and iron and manganese oxide and hydroxide. In addition to the triple lenses, small and medium veins and lenses of other types also outcrop in the area. Calamine lenses and veins are located at the central part and in K_a^{12} reefal-karstic unit, and have been specified as Zn-Pb^{ore} in the geological map, scale 1:1000 (Figure 2). Strike of mineralizations is in NW-SE direction, which conforms to the tectonic structures of the area such as folds, faults, and fractures. From the west, the calamine mine is encompassed by the main and important faults of the area called Black-Hill and from the east by North Forouzandeh [36, 38] (Figure 1). Silicification and iron oxide and hydroxide are among the observable alterations in this ore deposit (Figure 7). As a result of the activity of descending waters in ankerite dolomites, an iron-rich area has been created, which outcrops in yellowish brown to dark brown and red on the surface. Alteration of iron oxide includes minerals such as Siderite, Goethite, Hematite, and Limonite.
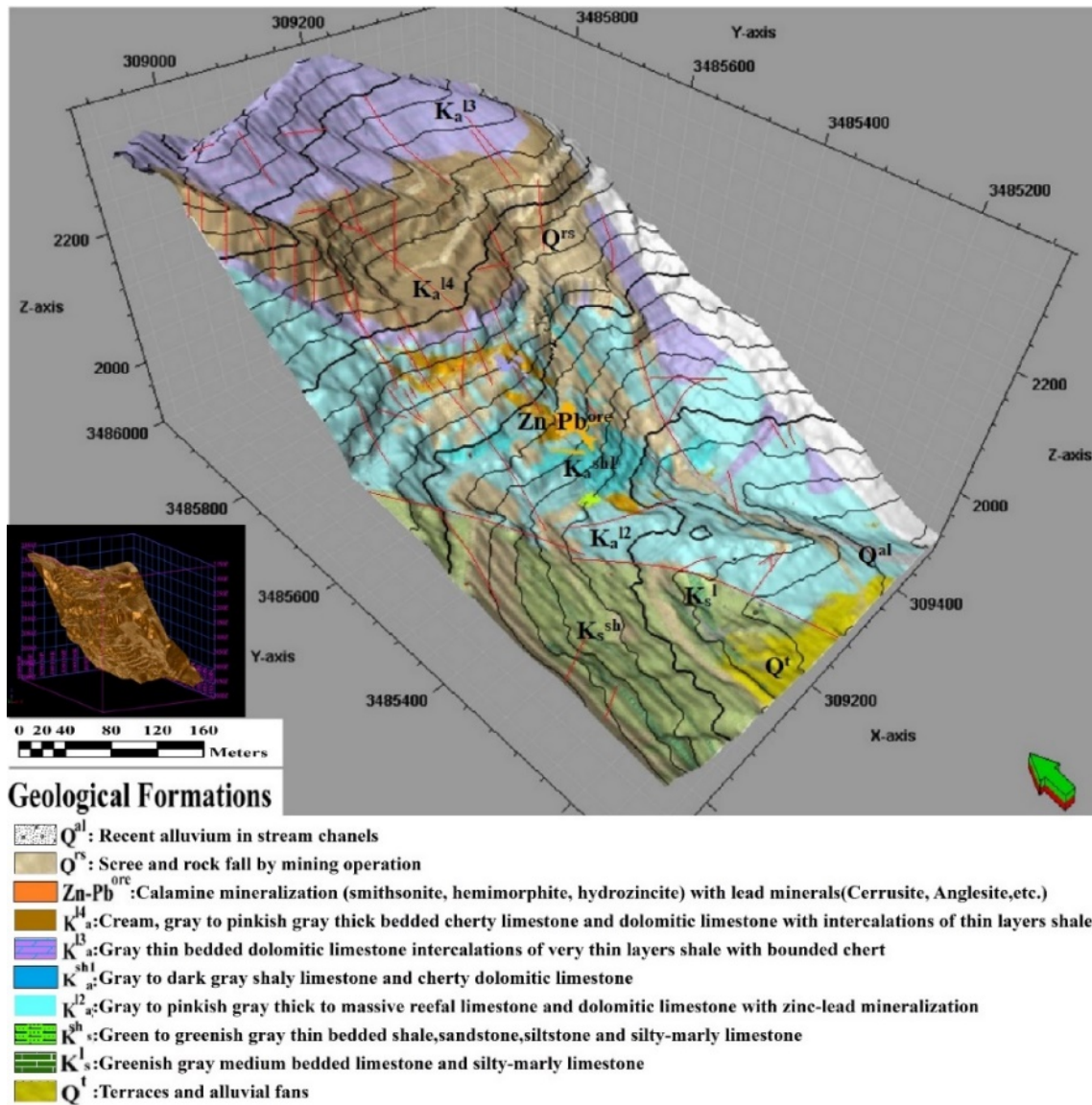
Geological Formations

⬚ Q^{al}: Recent alluvium in stream chanels

⬚ Q^{rs}: Scree and rock fall by mining operation

⬚ $Zn\text{-}Pb^{ore}$:Calamine mineralization (smithsonite, hemimorphite, hydrozincite) with lead minerals(Cerrusite, Anglesite,etc.)

⬚ K_a^{l4}:Cream, gray to pinkish gray thick bedded cherty limestone and dolomitic limestone with intercalations of thin layers shale

⬚ K_a^{l3}:Gray thin bedded dolomitic limestone intercalations of very thin layers shale with bounded chert

⬚ K_a^{sh1}:Gray to dark gray shaly limestone and cherty dolomitic limestone

⬚ K_a^{l2}:Gray to pinkish gray thick to massive reefal limestone and dolomitic limestone with zinc-lead mineralization

⬚ K_s^{sh}:Green to greenish gray thin bedded shale,sandstone,siltstone and silty-marly limestone

⬚ K_s^{l}:Greenish gray medium bedded limestone and silty-marly limestone

⬚ Q^{t}:Terraces and alluvial fans

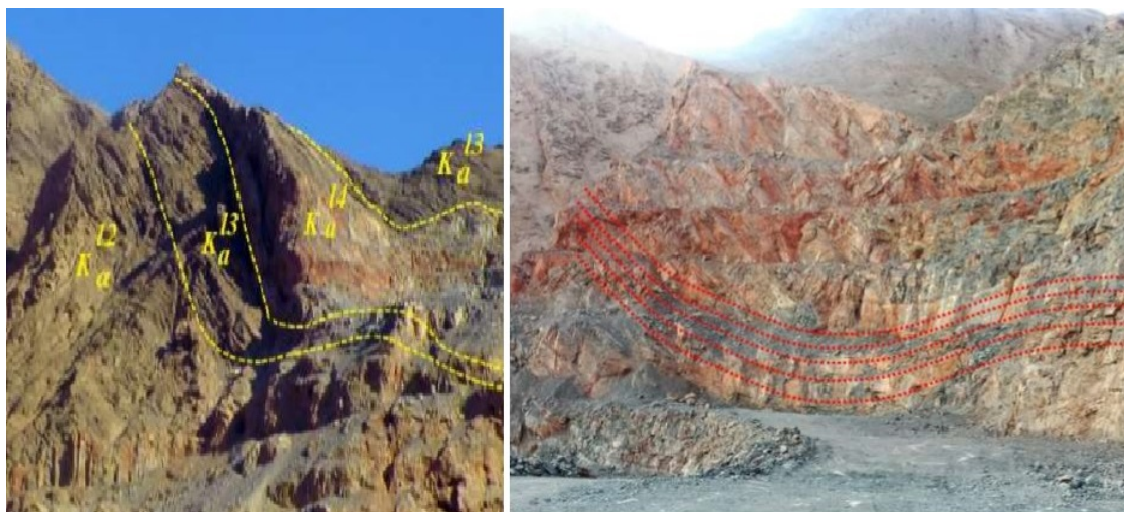**Figure 2. Geological map of Mehdiabad calamine (Scale 1:1000).**

Figure 3. Views of the outcrops of unit K_a^{l4} and its stratigraphic position relative to other rock units in the area.

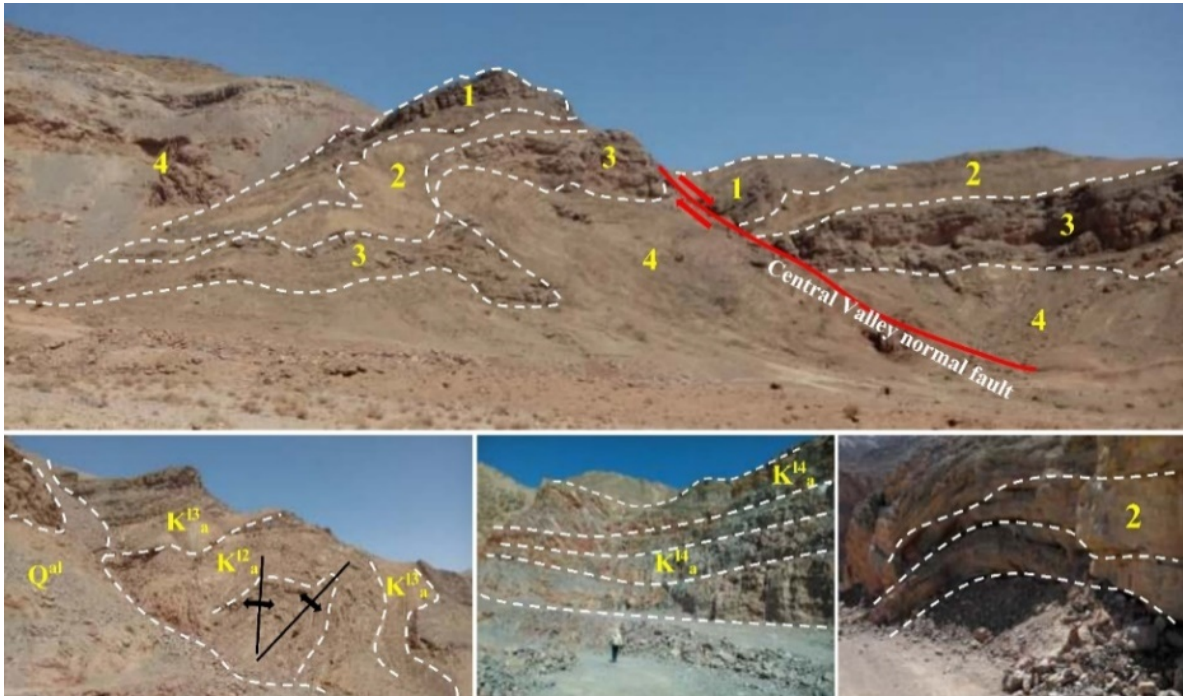**Figure 4. Views of the calamine rock unit folds and mineralization in the folded layers. 1: Chert-bearing bedded limestone 2: Limy shale and laminarlimestone 3: Reef limestone, porous limestone 4: Dolomitic shale, intercalation of chert. Q^{al}: River sediment.**
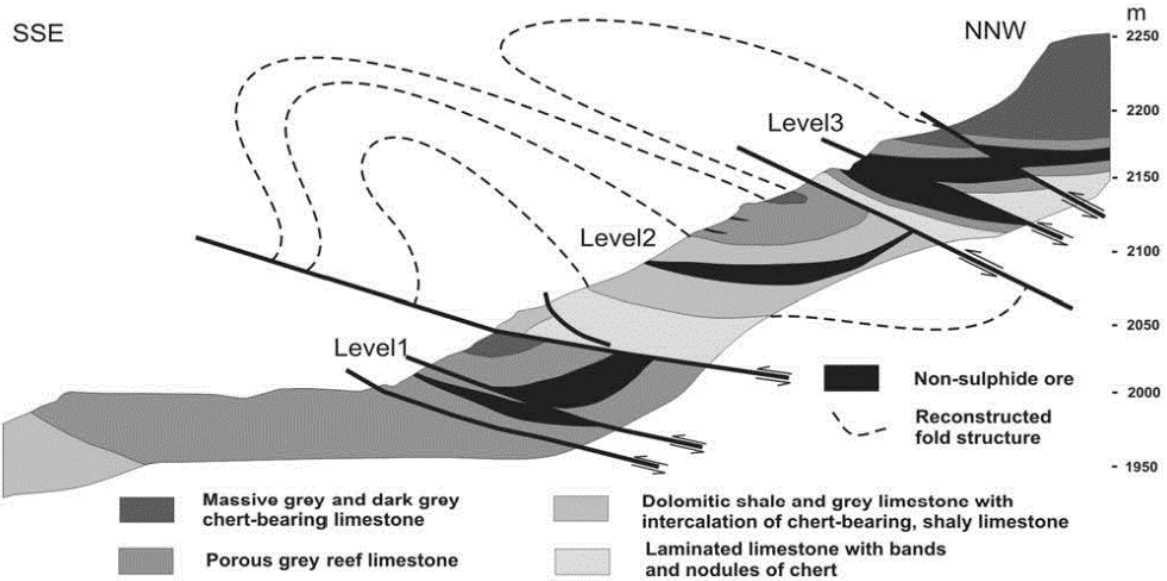

Figure 5. Schematic x-section NNW-SSE of the folded and faulted strata at the calamine mine area [36, 38].
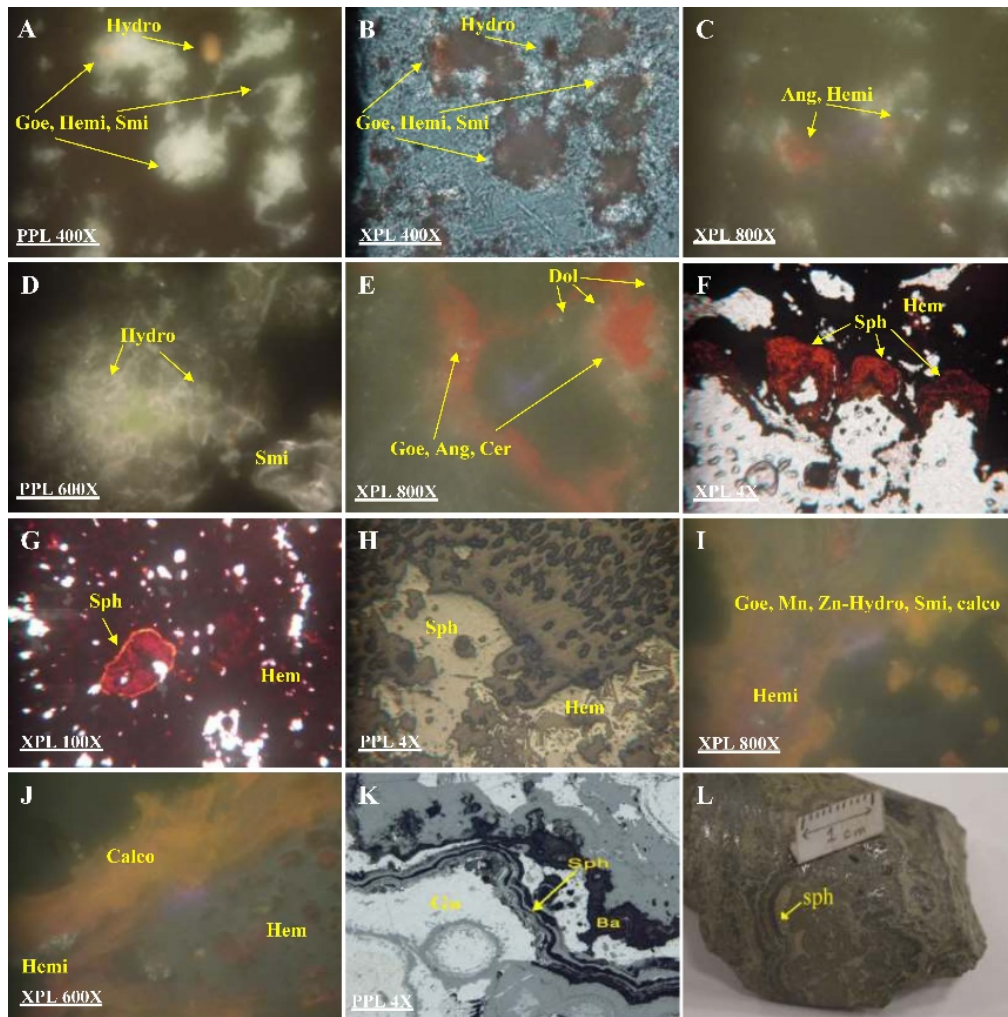
Figure 6. (A, B) Zinc minerals intergrowth consisting of smithsonite, hemimorphite, sulfide and silicate, hydrozincite with colloidal texture. Effects of goethite mineralization and iron oxide are observed (XPL, PPL 400X). (C) Formation of anglesite and hemimorphite minerals (XPL 800X). (D) Smithsonite mineral, colorless or faintly tinted in transmitted light and hydrozincite mineral (PPL 600X). (E) Goethite, anglesite and cerussite minerals (XPL 800X). (F) Formation of hematite and botryoidal mass minerals. Replacement of zinc, iron, and manganese around the sphalerite (XPL 4X). (G) Formation of sphalerite mineral with concentric chloroform texture, color change in different strips due to changes in the amount of iron (XPL 100X). (H) Replacing the goethite 'tooth-texture' has produced a pseudo-growth radially aligned pattern of fine hematite (PPL 4X). (I) and (J) Formation of hematite, calcophanite, hemimorphite, smithsonite and goethite. Substitution of the Zn and Mn elements in the hydrozincite (XPL 600, 800X). (K) Sphalerite mineral with concentric chloroform texture (Barite, Galena) (PPL 4X). (L) Sphalerite mineral with chloroform texture rock sample.
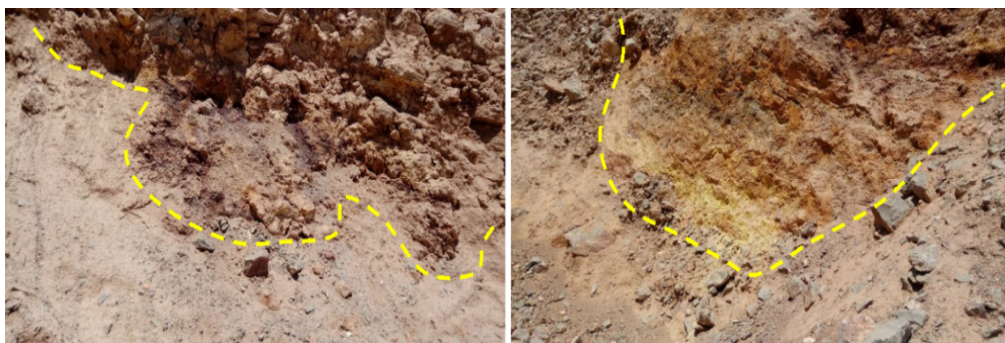

Figure 7. Remains of alterations and the only sulphoride areas left in the second lens of calamine mine.

4. Methodology
4.1. Vario-Fractal Modeling (a mathematical approach for geochemical explorations)

Mathematically, it is possible to define a function f(x) by considering two spatial-variables called x and y so that the variances between any two points x1, y1 and x2, y2 have a mean or expected value that increases as the square root of the vector distance between the two points. This is a two-dimensional BS. If the exponent of increase is different from 1/2, it is called a fractal BS [7, 13, 31, 43]. This equation was first introduced for the geomorphological investigations based on a power-law relationship between the variances of elevations versus the intervals of the variances [26]. Also the same variographic equation (Vario-Fractal) was used in order to analyze the independency of Bouguer anomalies from topographic gradients in SW of Iceland [27] as well as in Charak oil field of Iran after revising and conducting the compatibility check with the GIS software [43]. The Variance-Distance (V-D) equation is of fractal type, which indicates a power-law relationship between the variances of elevations (Vx), the distance of variances (intervals) (Dvx), and the fractal dimension (FD) as follows:

$$Vx = Dvx^{FD} \tag{1}$$

In order to convert Equation 1 to the vario-fractal equation (Equation 2), a logarithmic scale is necessary:

$$Log\ (Vx) = FD\ Log\ (Dvx) \tag{2}$$

where Log (Vx) and Log (Dvx) are the logarithms of variances of the points on contoured maps and the measured distances between them (variance intervals), respectively. Also FD is the fractal dimension. A log-log plot was utilized in order to illustrate the cumulative relation of Vx versus Dvx in the density functions [26, 27, 31]. "Spatial Analyst, SA", is a GIS-based software used to obtain the variance-distance equation through the fast and accurate interpolating algorithms [43-46]. This soft-package is a powerful tool for summarizing the statistical tables and communicating with other software applications such as Excel, used here to draw the vario-fractal diagrams. From a geostatistical viewpoint, the concept and the variability of this equation are similar to those of variographs. Therefore, the meaning of FD changes in BSs is similar to the meaning of semi-variograms to achieve the "range"

of a distribution. The distinction between these two algorithms lies in the self-organization of naturally occurring distributions, which can be identified based on the FD changes. By this definition, a self-organized pattern is the natural tendency of elements to migrate in the fluid Medias (such as hydrothermals) along with the multiplicative cascade processes [47]. Also it seems that a large scale diffusion-aggregation process results in the geochemical self-organization of elements in the primary stages of mineralization [31]. In the current research work, we used the V-D equation to optimize the variographic characteristics of elements according to fractal conceptual algorithms, which can be utilized to find geometric inter-relation of primary geochemical halos at logarithmic scales. In a geochemical dataset surveyed for purposes of ore-mineral explorations, a Brownian Surface (BS) is a fractional surface appearing in fractal density functions (on log-log plots) for delineation of the pattern of multiplicative cascade processes of ore-elements at the edge of chaotic distributions.

From the geochemical-fractal viewpoints, mineralization is a small but proper stage of numerous migration of elements and their crystallization from magmatic fluid-flows, which can be stated at 2 < FD < 3 [28]. For example, in the Queensland ore deposits, the noteworthy stages of gold mineralization are often syngenetic with quartz-colloform facies [48], and denote the relation between the ore-bearing processes and the non-linear texture growth during multiplicative cascade processes of epithermal systems [49]. In addition, it seems that in the epigenetic mineralization processes located in the marginal volcanic basins (e.g. SEDEX ore-deposits), most mineralized regions were characterized by self-organized elements in geometric correlation with BSs.

4.2. Research Methodology

Fractal Dimension (FD) is a parameter that is independent from the central tendencies as well as the distribution parameters, which for 2D arrays, denote self-similar peculiarities of distribution on BSs [7, 31]. In calamine, FD changes were calculated in order to achieve fractal surfaces of elements using a set of field data. Hence, a total of 180 litho-samples were collected and interpolated by the geostatistical techniques in order to determine the priority of geochemical zonation of indicator/pathfinder elements around ore-deposits. At first, the correlation and Poisson distribution

coefficients were calculated and illustrated by the data in Table 1 for the set of indicator and pathfinder elements.

In this table, Pb has linear correlations with Ag, Sb, Fe, and Cd, and Zn has the same correlations with Sb, Cd, Fe, Ni, Pb, and As. The relation of the main ores (Zn and Pb) with trace elements is of a linear type, proportioned to As, Sb, and Fe contents for Pb mineralization, as well as to Sb, Cd, Fe, and Ni contents for Zn. Although the increase in correlation coefficients can be interpreted as a

closer relationship of elements, their dependency on sampling procedures as well as distribution parameters increase the BIAS during non-systematic surveys (discrete sampling). Presuming this and owing to the Poisson distribution of elements (Table 1), it seems that replacing the linear results with fractals is a necessary approach for a BIAS decrease and evaluating the tendency of elements to self-organize in the volcanogenic environments.

Table 1. Correlation coefficient and possibility of Poisson distribution indicator and pathfinder elements of calamine mine (λ: expected mean; λ1: background; λ2: anomalies).

		Supra-ore elements						Redox elements			Sub-ore elements			
		Pb	**Zn**	**Ag**	**Sb**	**As**	**Ba**	**Fe**	**S**	**Cd**	**Cu**	**Ni**	**Co**	**Cr**
Correlation Coef.	Pb	1.00	0.57	0.57	0.81	0.39	0.24	0.79	0.41	0.54	0.06	0.31	0.19	0.12
	Zn	0.57	1.00	0.22	0.75	0.55	0.42	0.65	0.35	0.66	0.02	0.62	0.38	0.11
Poisson dist. Coef.	λ1	0.30	0.38	0.74	0.38	0.45	0.44	0.40	0.40	0.30	0.53	0.55	0.65	0.53
	λ2	0.35	0.73	0.29	0.51	0.60	0.45	0.42	0.30	0.37	0.31	0.41	0.53	0.37

In this research work, a V-D equation (Eq. 2) was applied in order to modify the linear regression results. This equation is a logarithmic expression for revealing BSs as the geometric features related to geochemical zonation of elements at the edge of chaos [7]. The presence and continuity of fractal surfaces are scale-invariance, in the range of 2.5 > FD > 2 [27]. Accordingly, a Brownie surface indicates a realized tendency of elements toward a non-linear distribution, which is usually related to the initialized/primary stages of mineralization in deeper/hypogene environments [49-51]. In the geochemical exploration, BS correlation represents a series of paragenetic elements that exist in the presence of each other, as expected in the hypogene environments. Comparison of the regression coefficient values (Table 1) with FD changes, as can be seen in Table 2, indicates the reliability of the vario-fractal equation in realizing geochemical zonation of elements in the calamine region. In order to find the precursor role of trace-elements, their geochemical inter-relations must be stated by the power-law function, where the measured intervals (Dvx) are a function of calculated variances (Vx). Thereby, after interpolating the gradient values of elements, the fractal surfaces can be delineated on logarithmic diagrams for prioritizing the mineralization potentials based on the zonation of elements.

5. Results and Discussions

Obtaining the BSs of elements as non-linear evaluation criteria for mineralization potentials is a new hypothesis, proposed here for the purpose of prospecting ore minerals in the calamine region. Accordingly, Pb, Zn, Sb, Ag, As, and Ba were considered as supra-elements, while Cu, Co, Ni, Cr, and Cd were regarded as sub-ores. In addition, Fe and S were discussed as two redox elements, as follow:

5.1. Analyzing Fractal Surfaces of Elements
A. Ores with Real BSs

A.1. Pb (supra-ore indicator): According to Table 2, a real Brownie has appeared in Pb at FD = 2.15 by measuring the gradient of concentration (28382 to 33466 ppm) at 17 to 21 m away from the center of anomaly (38657 ppm). As depicted in Figure 8A, Pb anomaly is of a limited self-organized type, denoting an intrinsic correlation with calamine's geochemical zonation (CGZ) as a local indicator.

A.2. Zn (supra-ore indicator): According to Table 2, a real Brownie has appeared in Zn at FD = 2.68 by measuring the gradient of concentration (24619 to 33495 ppm) at 52 to 98 m away from the center of anomaly (38480 ppm). As depicted in Figure 8A, Zn anomaly is of an extended self-organized type, denoting an intrinsic correlation with CGZ as a regional indicator.

A.3. Sb (supra-ore pathfinder): According to Table 2, a real Brownie has appeared in Sb at FD = 2.63 by measuring the gradient of concentration (267 to 2169 ppm) at 37 to 65 m away from the center of anomaly (128 ppm). As depicted in Figure 8A, Sb anomaly is of a real and extended self-organized type, denoting intrinsic correlation with CGZ as a regional pathfinder.

A.4. Ag (supra-ore indicator): According to Table 2, a real Brownie has appeared in Ag at FD = 2.02 by measuring the gradient of concentration (508 to 1062 ppm) at 15 to 17 m away from the center of anomaly (63 ppm). As depicted in Figure 8B, Ag threshold is of a limited self-organized type, denoting an intrinsic correlation with CGZ as a local indicator.

A.5. Cu (sub-ore pathfinder): According to Table 2, a real Brownie has appeared in Cu at FD = 2.14 by measuring the gradient of concentration (79 to 115 ppm) at 19 to 29 m away from the center of anomaly (121 ppm). As depicted in Figure 8B, Cu anomaly is of a limited self-organized type, denoting an intrinsic correlation with CGZ as a local pathfinder.

A.6. Co (Sub-ore pathfinder): According to Table 2, a real Brownie has appeared in Co at FD = 2.05 by measuring the gradient of concentration (11 to 16 ppm) at 23 to 32 m away from the center of anomaly (21 ppm). As depicted in Figure 8B, Co threshold is of a limited self-organized type, denoting a deeper intrinsic correlation with CGZ as a local pathfinder.

A.7. Ni (Sub-ore pathfinder): According to Table 2, a real Brownie has appeared in Ni at FD = 2.31 by measuring the gradient of concentration (55 to 76 ppm) at 14 to 18 m away from the center of anomaly (87 ppm). As depicted in Figure 8C, Ni anomaly is of limited self-organized type, denoting a deeper intrinsic correlation with CGZ as a local pathfinder.

A.8. Cr (independent sub-ore element): According to Table 2, two real Brownies have appeared in Cr at FD = 2.69 and FD = 2.71 by measuring the gradient of concentration (14 to 37 ppm) at 67 to 163 m away from the center of anomaly (50 ppm). As depicted in Figure 8C, although Cr threshold is of an extended self-organized type, it is uncorrelated with CGZ geometrically.

Table 2. V-D model for metals with Real BSs (FD: Fractal Dimension, BS: Brownian Surface, Var: Variance, D: Distance (m), Dn-Dmin: Differential Distance (m), Cum Area: Cumulative Area).

Element	Cum area	D (m)	Dn-Dmin	Grade (ppm)	Var	Log (Dn-Dmin)	Log (Var)	Slope	FD	BS
Pb	1375	20.93	8.00	28382.43	105578715.74	0.90	8.02	2.15	2.15	Real
	925	17.16	4.233	33466.10	26951468.74	0.63	7.43			
Zn	30225	98.11	85.18	24619.84	192125751.94	1.93	8.28	2.29	2.68	Real
	18025	75.77	62.84	28698.96	95684086.64	1.80	7.98	2.90		
	8625	52.41	39.48	33495.98	24848277.90	1.60	7.40			
Sb	13550	65.69	52.76	81.52	2169.24	1.72	3.34	3.18		
	9425	54.79	41.86	95.85	1039.62	1.62	3.02	2.46	2.63	Real
	4300	37.01	24.08	111.76	266.84	1.38	2.43	1.76		
Ag	900	16.93	4.00	30.96	1062.94	0.60	3.03	2.03	2.03	Real
	350	15.71	2.78	41.01	508.62	0.44	2.71	0.95		
Cu	2700	29.32	16.39	79.0651	2236.33	1.21	3.35	2.27		
	1800	23.94	11.01	98.2484	906.41	1.04	2.96	2.06	2.14	Real
	1175	19.34	6.41	115.1245	296.89	0.81	2.47	3.06		
Co	3300	32.42	19.49	11.33	97.24	1.29	1.99	1.91		
	2350	27.36	14.43	13.80	54.67	1.16	1.74	2.17	2.05	Real
	1700	23.27	10.34	16.04	26.52	1.01	1.42	2.44		
Ni	1025	18.07	5.14	55.09	1021.90	0.71	3.01	1.66		
	825	16.21	3.28	65.05	484.46	0.52	2.69	2.05	2.31	Real
	675	14.66	1.73	76.47	112.02	0.24	2.05			
Cr	52575	129.40	129.40	21.08	861.56	2.11	2.94	1.08	2.69	Real
	22550	84.74	71.81	32.68	315.01	1.86	2.50	2.63	2.71	Real
	14450	67.84	54.91	37.95	155.64	1.74	2.19	1.70		

B. Non-Ores with Real BSs

B.1. As (precursor pathfinder): According to Table 3, a real Brownie has appeared in As at FD = 2.63 by measuring the gradient of concentration (84 to 112 ppm) at 94 to 179 m away from the center of anomaly (130 ppm). As depicted in Figure 8D, As anomaly is of an extended self-organized type, denoting an intrinsic correlation with CGZ as a proper regional pathfinder.

B.2. S (redox indicator): According to Table 3, a real Brownie has appeared in S at FD = 2.20 by measuring the gradient of concentration (24393 to 33482 ppm) at 24 to 40 m away from the center of anomaly (38710 ppm). As depicted in Figure 8D, S anomaly is of a limited self-organized type, which may locally be related to the redox condition of CGZ.

Table 3. V-D model for non-metals with Real BSs (FD: Fractal Dimension, BS: Brownian Surface, Var: Variance, D: Distance (m), Dn-Dmin: Differential Distance (m), Cum Area: Cummulative Area).

Element	Cum area	D (m)	Dn-Dmin	Grade (ppm)	Var	Log (Dn-Dmin)	Log (Var)	Slope	FD	s
As	100650	179.04	166.11	84.8843	2013.48	2.22	3.30	2.50		
	61425	139.86	126.93	97.7117	1026.84	2.10	3.01	2.76	2.63	Real
	27750	94.01	81.08	112.4831	298.36	1.91	2.47	1.30		
S	5175	40.60	27.67	24393.12	204992930.97	1.44	8.31	2.24		
	3300	32.42	19.49	29047.86	93370360.91	1.29	7.97	2.34	2.20	Real
	1900	24.60	11.67	33483.00	27328838.93	1.07	7.44			

C. Ores with Near BSs

C.1. Cd (sub-ore pathfinder): According to Table 4, a near Brownie has appeared in Cd at FD = 1.67 by measuring the gradient of concentration (397 to 339 ppm) at 14 to 16 m away from the center of anomaly (449 ppm). As depicted in Figure 8E, Cd anomaly is of a limited quasi-fractal type, although it indicates a relative geometric correlation with CGZ as a local pathfinder.

C.2. Fe (redox indicator): According to Table 4, a near Brownie has appeared in Fe at FD = 1.83 by measuring the gradient of concentration (94961 to 111952 ppm) at 22 to 33 m away from the center of anomaly (129044 ppm). As depicted in Figure 8E, Fe anomaly is of a limited quasi-fractal type, which may locally be related to the redox condition of CGZ.

Table 4. V-D model for metals with Near BSs (FD: Fractal Dimension, BS: Brownian Surface, Var: Variance, D: Distance (m), Dn-Dmin: Differential Distance (m), Cum Area: Cummulative Area).

Element	Cum area	D (m)	Dn-Dmin	Grade (ppm)	Var	Log (Dn-Dmin)	Log (Var)	Slope	FD	BS
Cd	850	16.45	3.52	339.38	12210.69	0.55	4.09	1.67	1.67294	Near
	650	14.39	1.46	397.07	2789.11	0.16	3.45			
Fe	3575	33.74	20.81	94961.56	1161622129.94	1.32	9.07	1.84		Near
	1625	22.75	9.82	111952.76	292115366.02	0.99	8.47			

D. Non-Ores with Near BSs

D.1. Ba (precursor pathfinder): According to Table 5, a near Brownie has appeared in Ba at FD = 1.60 by measuring the gradient of concentrations (7939 to 11178 ppm) at 14 to 19 m away from the center of anomaly (12619 ppm). As depicted in Figure 8F, Ba anomaly is of a limited quasi-fractal type, indicating its lack of precursory for other elements.

Table 5. V-D model for non-metals with Near BSs (Ba) (FD: Fractal Dimension, BS: Brownian Surface, Var: Variance, D: Distance (m), Dn-Dmin: Differential Distance (m), Cum Area: Cummulative Area).

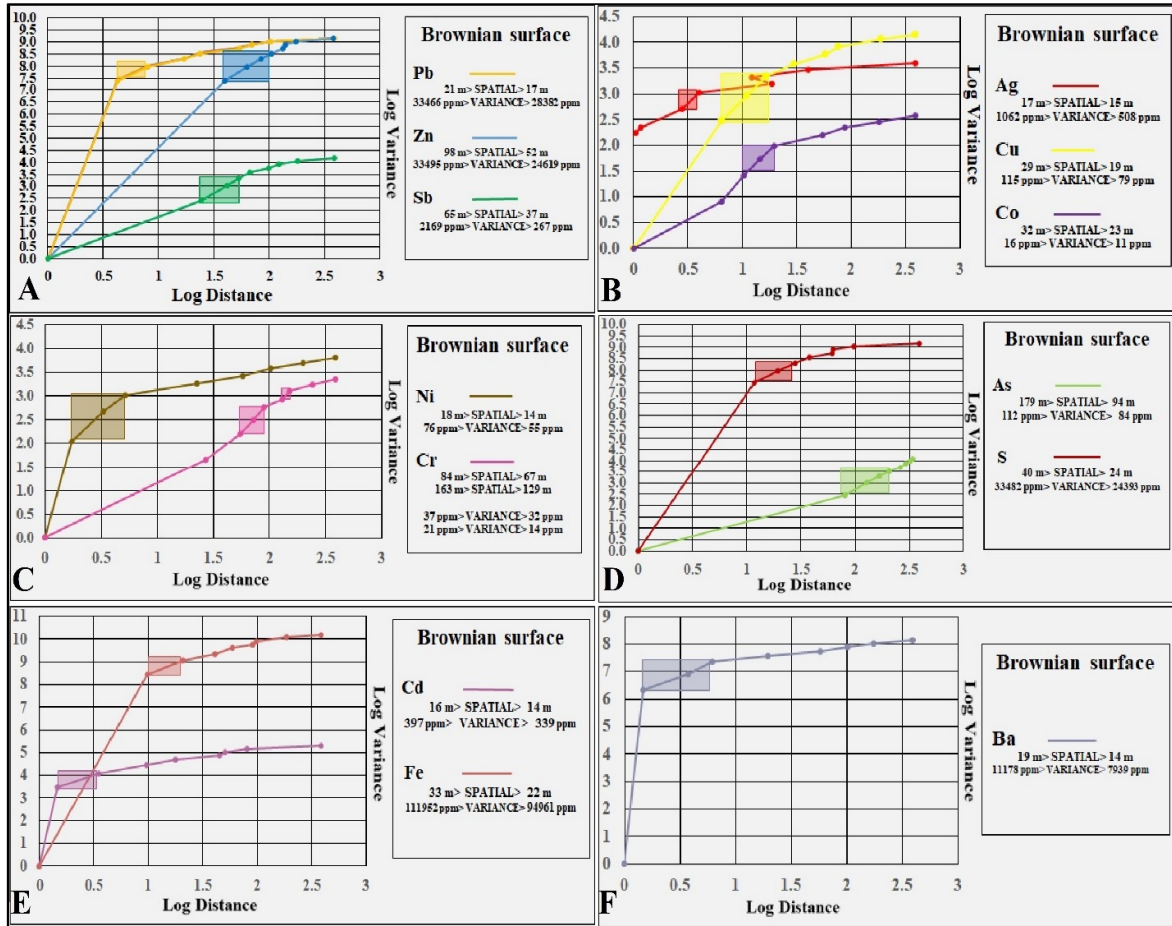| Cum area	D (m)	Dn-Dmin	Ba (ppm)	Var (Ba)	Log (Dn-Dmin)	Log (Var)	Slope	FD	BS
1150	19.14	6.21	7939.64	21903002.79	0.79	7.34	1.95		
875	16.69	3.76	9745.74	8259701.84	0.58	6.92	1.46	1.60344	Near
650	14.39	1.46	11178.65	2076655.36	0.16	6.32			

Figure 8. V-D density function for pathfinder elements of calamine (13 element). Blue indicates real BS and green indicates near BS.

5.2. Priorities of Target-Areas for Prospection

Calamine PGZE has been prioritized in 6 target areas (shown in Figure 9) for further prospection by comparing BSs of elements, summarized in Figure 8. Accordingly, the suitability of geochemical distribution patterns depends on the presence and the orderly zoning of As, Zn, Cr, Sb, S, Co, Cu, Pb, Ni, and Ag. Also for other pathfinder elements (Fe, Ba, and Cd), the distribution patterns are of quasi-fractal types, appearing in near Brownies. For the series of paragenetic elements, a proper and orderly zonation, as expected in fractal geometry, should be specified by inter-relation of elements within self-organized populations [49]. Apart from the priorities of calamine ore-bearing geological formations, arsenic has the largest Brownie, while the smallest one belongs to Ag and Cd. Among the elements that have naturally reached their BSs (Figure 9), As, Sb, and Zn have the same parameters in FDs and self-similar populations. The above-mentioned elements have been extended well in the background of other

elements, representing the presence and effect of post-magmatic stages of mineralization. Cr is the only independent element whose Brownie has no correlation with Brownies of As, Pb, and Zn. Owing to the inter-relation of fractal surfaces, 6 target areas, as summarized in Figure 9, are introduced as follow:

Target No.1 (T1): Here, an effective correlation can be seen between As, Sb, Pb, Zn, Ag, and Cd. All surfaces are of fractal types (Brownie at FD > 2). The maximum Ag content is at the point where it overlaps with Pb. Presence of various Brownies and their proper correlations with each other is a good zoning indication of elements at T1 (priority No.1 for Zn and Pb exploration).

Target No. 2 (T2): Here, another effective correlation can be seen between As, Sb, Pb, and Zn. Also Pb has a partial correlation with Fe due to the iron's quasi-fractal distribution. The lack of sulfur's fractal distribution indicates a dominant oxidizing condition. Like T1, the presence of BSs and their correlation with each other is an indication of the

relative zoning of elements. However, in the absence of Cd, the concealed mineralization potential of Zn may be decreased.

Target No. 3 (T3): Here, in addition to a set of supra-ore elements (Pb, Zn, As, Sb, Ba), two middle-ores (Cd, Cu) and one sub-ore (Ni) plus iron are in an efficient correlation with each other. Except for As and Ba, self-similar population of Pb is independent from the others. Although fractal distribution and Pb-Cd relation is the same as T1, in the absence of Pb, the relative correlation of middle-ores can be utilized for deeper explorations.

Target No. 4 (T4): Here, another set of the elements including Zn, As, and Sb, as supra-ore elements, Cu, as middle-ore element, and Ni and Co, as sub-ore elements can be seen in correlation with S as a redox element. Additionally, since T4 has S and lacks Pb, it shows a possible enriched zone under the erosion shearing surface.

Target No. 5 (T5): Here, the fractal distribution of elements is like the one for T1, and the discrepancy is that T5 lacks BSs of Cd and Ag, representing a closer proximity to the erosion shearing surfaces (note that Ag is present but never reaches a fractal surface).

Target No. 6 (T6): Here, the fractal distribution of elements is significantly similar to that of T4. The only difference is that T6 lacks a Co's Brownie, while for Ni, it is developed just as in Cd and Fe. Moreover, a geometric proximity between Fe and S represents the overall redox condition of this area.
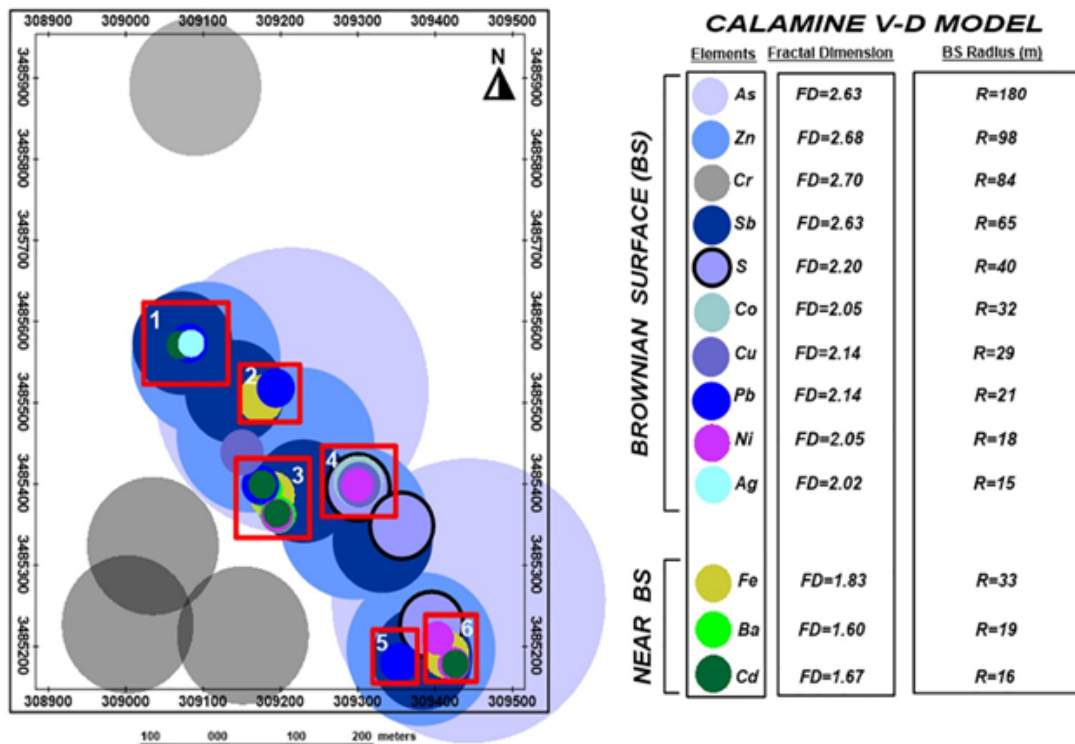

Figure 9. Prejudice map obtained from the V-D model in the calamine mine of Mehdiabad, Yazd. The geometric location of BSs is circular to represent a symmetrical distribution of self-similarities on fractal surfaces. According to FD variations, the first 10 elements have real BSs, while the last 3 elements contain near BSs.

5.3. Mineralogical evidences of PGZE

Considering the redox condition discrepancy between T2 and T4 and owing to the sphalerite mineralization distinction at T4 (Eh < 0) is opposite to the paragenesis of hemimorphite-goethite at T2 (Eh > 0). Overall, 4 litho-samples from T2 and T4 were taken and prepared in order to mark the advantage of vario-fractal modeling to predict hypogenic potential of mineralization by means of primary geochemical pattern recognition in the surficial halos (Figure 10). Owing to a considerable sphalerite phenocrysts (micrographs: A and B), T4 has a sulfide-rich mineralogical aggregation, as expected in the SEDEX deposits, which is in accordance with fractal evidence of PGZE (see Figure 10). On the other hand, T2 has no sulfide minerals, which dominantly consist of hemimorphite mega crystals in the ground of quartz and gypsum, although it may be replaced by hematite-goethite and smithsonite under surficial oxidizing conditions simultaneously (micrographs:

C and D). From both the mineralogical and vario-fractal viewpoints, T4 has a better aggregation of sulfide-rich ore minerals than T2, and according to

the non-linear analysis of geochemical dataset, T4 contains a better PGZE than T2.
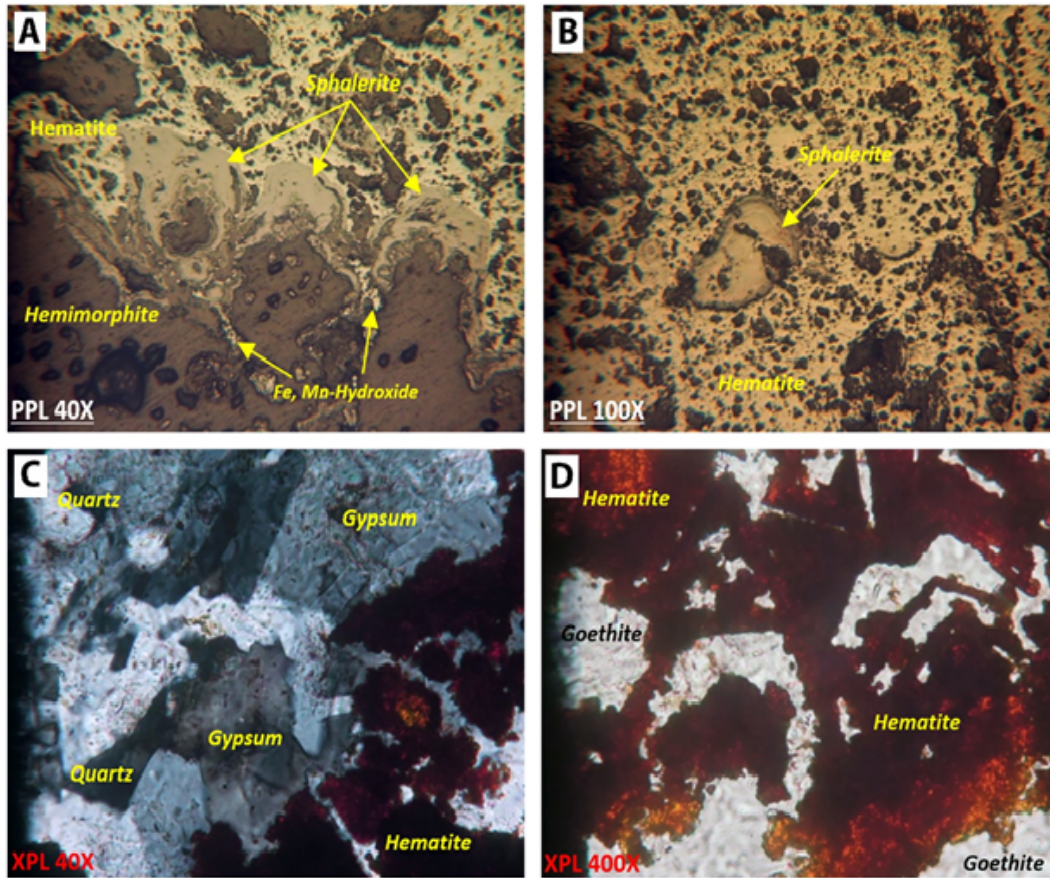

Figure 10. The mineralogical aggregation of Zn and Fe ores among the reducing and oxidizing conditions of T4 and T2, respectively.

6. Conclusions

In this paper, the first emphasis was on the delineation of Brownian surfaces of the calamine's typomorphic elements using the vario-fractal equation. Where an element is in a self-organizing condition, its Brownie can be regarded as a new geometric criterion for inter-relation with other elements. In such a case, the Brownies contain a set of self-similar populations that may locally be correlated with primary zonation of ore elements due to the deep mineralization processes. According to Table 1 and Figure 8, the results of comparisons of the correlation coefficients of the calamine's typomorphic elements with the FD changes are as follow:

- Comparison of the Pb and Zn correlation coefficients with those of Fe, Sb, Ni, and Cd indicates paragenesis of the main ores with a number of pathfinder elements. Meanwhile, a tendency towards exponential distribution can be

expected for the elements that have a Poisson distribution. Accordingly, it cannot be claimed that the calamine's geochemical zonation can be realized well using a simple Poisson distribution; rather, it can be claimed that the vario-fractal equation reduces the random diffusive effects in geochemical zonation by geometric delineation of BSs.

- BSs of As, Sb, Zn, and Cr are of extended types in contrast with Pb, Ag, Cu, Ni, and S, which are of limited types. Moreover, Fe, Ba, and Cd well-appear in near Brownies as representing quasi-fractal populations ($1.5 > FD < 2$). Hence, 10 elements of the 13 selected elements reached an optimum FD ($3 > FD > 2$), which probably coincided with the mineralization events but the other three elements with $FD < 2$ appeared in quasi-fractal populations ($1.5 > FD < 2$).
- Comparison of the fractal surfaces of Cd and Ba with real Brownies of other elements reveals their spatial relations with the underlying mineralization of Pb and Zn.

- Iron's correlation coefficient has a significant difference with its FD, and indicates that this element, rather than being a pathfinder element, represents the redox condition of the geochemical environment.

- Comparison between the correlation coefficient and FD changes of Cr indicates that its Brownie extended well without geometrically overlapping with other elements. This means that the relevant sources to Cr fractal distribution are geochemically different from other sub-ores of the region.

The second emphasis in this paper was on introducing a vario-fractal model to reveal geochemical zonation of 13 indicator and pathfinder elements in six target areas located in the central and southwestern part of the calamine region, as shown in Figure 9. Applications and advantages of this model are as follow:

- Zinc mineralization is a noteworthy potential in all 6 targets as, compared to Pb, it has a more extended BS and a relatively unified distribution level. On the other hand, the Pb potential seems to be limited to T1, T2, T3, and T5, where it is properly correlated with BS of Zn.

- In the vario-fractal modeling, the recognition and prioritization of pathfinder elements are conspicuously different from those used in the linear models.

- Considering the correlation coefficient of elements, Ag is a footprint of possible Pb-Ag mineralization in the T1 depth. Moreover, the correlation between BSs of Ag and Pb is optimum, giving rise to the same result as in the linear methods. Since in T1 the Ag content has reached an optimum FD, its geochemical zonation can be utilized for correlation with other elements such as Pb; this is while Ag lacks this condition in other promising areas, and consequently, does not have any suitability for path-finding.

- Owing to the Brownies of Ag and Cd and their correlation with fractal surfaces of other indicators, the non-linear distribution of elements, with emphasis on Pb, is well self-organized in T1 and T5, and denotes their advantages for a deep mineralization exploration.

- For T4 and T6, the position of Brownies for Fe and S may locally indicate the continuity of Zn mineralization under the redox conditions. Also the presence of sulfur zonation and its constraint on T4 and T6 indicates geochemical distributions under the reducing conditions. Unlike iron, the sulfur's FD is optimum and correlates with Brownies of Sb, Zn, Ni, and Co geometrically.

- In contrast to T4 and T6, the redox pathfinders of T2 and T3 have appeared in near Brownies under the oxidizing conditions. Since the increase in the random FDs is due to stochastic processes of supergene environments, the T2 and T3 stochastic distances were estimated at 60 to 80 m off the center of Fe distribution as surficial radius of erosion shearing of geochemical anomalies in a non-sulfide mineralization event.

- Owing to the precursory role of As in hydrothermal deposits, the Pb mineralization event is potentially related to T1, T2, T3, and T5. Also the potential of T1, T4, and T6 for Zn mineralization is more than in the other target areas. By an enrichment assumption, under the reducing conditions, T4 and T6 can be suggested for a further deeper exploration.

- Nickel's Brownie is extended well in T4, T6, and T3 and so displays an orderly zonation to accompany other elements. T4's Brownies of Ni, Co, Cu, and Zn are in optimum ranges, well overlapped with each other, which is indicative of more chances of exploration.

- The final model illustrates the importance of FD changes in geochemical setting of the calamine's non-sulfide ore-deposit quite well. Since this is the first time this model is being applied, the differences between the linear regression results and the current fractal model can be considered as a criterion for modifying the concept of mineralization as well as revising the priorities of explorations. In fact, this is a geometric pattern for recognition of orderly distribution of elements in the central and southeastern parts of calamine in such a way that spatio-temporal zonation of elements correlate with particular sequences of Cretaceous formations as mineralization of host units. This may lead to the conclusion that the calamine's mineralization event, as expected in the SEDEX ore-deposits, is not of a surficial type due to paragenetic elements' self-organization and their geometric correlations with each other. At the end, it should be noted that using linear approaches, realizing such a scale-invariant zonation of elements explained here for hydrothermal mineralization under random diffusive condition and multiplicative cascade processes of exhalative phases is quite impossible.

References

[1]. Borg, G., 2005. Geological and economic significance of supergene non-sulfide zinc deposits in Iran and their exploration potential. In: Geological Survey of Iran (Ed.) Mining and Sustainable Development. 20th World Mining Congress, Tehran, Iran. 7-11.

[2]. Grigoryan, S.V., 1974. Primary geochemical halos in prospecting and exploration of hydrothermal deposits. International Geology Review. 16(1), 12-25. https://doi.org/10.1080/00206817409471901.

[3]. Hitzman, M.W., Reynolds, N.A., Sangster, D.F., Allen, C.R., Carmen, and C.E., 2003. Classification, genesis, and exploration guides for non-sulfide zinc deposits. Economic Geology, 98(4), 685–714. https://doi.org/10.2113/gsecongeo.98.4.685.

[4]. Emsbo, P., 2009. Geologic Criteria for the Assessment of Sedimentary Exhalative (Sedex) Zn-Pb-Ag Deposits. U.S. Geological Survey, Reston, Virginia. Open-File Report, 21 pp.

[5]. Turcotte, D.L., 2002. Fractals in petrology. Lithos, 65(3-4), 261–271. https://doi.org/10.1016/S0024-4937(02)00194-9.

[6]. Maleki, M. and Emery, X., 2020. Geostatistics in the presence of geological boundaries: Exploratory tools for contact analysis. Ore Geology Reviews. 120, 103397. https://doi.org/10.1016/j.oregeorev.2020.103397.

[7]. Mandelbrot, B.B., 1983. The Fractal Geometry of Nature. W. H. Freeman, San Fransisco, 468 pp.

[8]. Barnsley, M.F., Devaney, R.L., Mandelbrot, B.B., Peitgen, H.O., Saupe, D., and Voss, R.F., 1988. The Science of Fractal Images. Springer-Verlag, New York, 327 pp.

[9]. Turcotte, D.L., 1997. Fractals and Chaos in Geology and Geophysics. Cambridge University Press, 414 pp.

[10]. Mehrnia, S.R., 2009. Using Fractal Filtering Technique for Processing ETM Data as Main Criteria for Evaluating Gold Indices in North West of Iran. International Conference on Computer Technology and Development, Kota Kinabalu, Malaysia, 379–393. https://doi.org/10.1109/ICCTD.2009.29.

[11]. Cheng, Q., 2012. Singularity theory and methods for mapping geochemical anomalies caused by buried sources and for predicting undiscovered mineral deposits in covered areas. Journal of Geochemical Exploration. 122, 55-70. https://doi.org/10.1016/j.gexplo.2012.07.007.

[12]. Nazarpour, A., 2018. Application of C-A fractal model and exploratory data analysis (EDA) to delineate geochemical anomalies in the: Takab 1:25,000 geochemical sheet, NW Iran. Iranian Journal of Earth Sciences. 10, 173–180.

[13]. Parsa, M., Maghsoudi, A., Yousefi, M., and Carranza, E.J.M., 2017. Multifractal interpolation and spectrum-area fractal modeling of stream sediment geochemical data: Implications for mapping exploration targets. Journal of African Earth Sciences. 128, 5-15. https://doi.org/10.1016/j.jafrearsci.2016.11.021.

[14]. Behera, S., Panigrahi, M.K., and Pradhan, A., 2019. Identification of geochemical anomaly and gold potential mapping in the Sonakhan Greenstone belt, Central India: An integrated concentration-area fractal and fuzzy AHP approach. Applied Geochemistry. 107, 45-57. https://doi.org/10.1016/j.apgeochem.2019.05.015.

[15]. Ghezelbash, R., Maghsoudi, A., and Carranza, E.J.M., 2019. Mapping of single- and multi-element geochemical indicators based on catchment basin analysis: Application of fractal method and unsupervised clustering models. Journal of Geochemical Exploration. 199, 90-104. https://doi.org/10.1016/j.gexplo.2019.01.017.

[16]. Liu, Y., Zhu, L., Ma, Sh., Guo, F., Gong, Q., Tang, Sh., Gopalakrishnan, G., and Zhou, Y., 2019. Constraining the distribution of elements and their controlling factors in the Zhaojikou Pb–Zn ore deposit, SE China, via fractal and compositional data analysis. Applied Geochemistry. 108, 104379. https://doi.org/10.1016/j.apgeochem.2019.104379.

[17]. Pourgholam, M.M., Afzal, P., Yasrebi, A.B., Gholinejad, M., and Wetherelt, A., 2021. Detection of geochemical anomalies using a fractal-wavelet model in Ipack area, Central Iran. Journal of Geochemical Exploration 220, 106675. https://doi.org/10.1016/j.gexplo.2020.106675.

[18]. Zuo, R., Xia, Q., Wang, H., 2013. Compositional data analysis in the study of integrated geochemical anomalies associated with mineralization. Applied Geochemistry. 28, 202-211. https://doi.org/10.1016/j.apgeochem.2012.10.031

[19]. Afzal, P., Heidari, S.M., Ghaderi, M., and Yasrebi, A.B., 2017. Determination of mineralization stages using correlation between geochemical fractal modeling and geological data in Arabshah sedimentary rock-hosted epithermal gold deposit, NW Iran. Ore Geology Reviews. 91, 278-295. https://doi.org/10.1016/j.oregeorev.2017.09.021.

[20]. Li, Ch., Ma, T., and Shi, J., 2003. Application of a fractal method relating concentrations and distances for separation of geochemical anomalies from background. Journal of Geochemical Exploration, 77(2-3), 167-175. https://doi.org/10.1016/S0375-6742(02)00276-5.

[21]. Hassanpour, Sh. and Afzal, P., 2013. Application of concentration–number (C–N) multifractal modeling for geochemical anomaly separation in Haftcheshmeh porphyry system, NW Iran. Arabian Journal of Geosciences. 6(3), 957-970. https://doi.org/10.1007/s12517-011-0396-2.

[22]. Farahmandfar, Z., Jafari, M.R., Afzal, P., and Ashja Ardalan, A., 2020. Description of gold and copper

anomalies using fractal and stepwise factor analysis according to stream sediments in NW Iran. Geopersia. 10(1), 135-148. Doi: 10.22059/geope.2019.265535.648413.

[23]. Daneshvar Saein, L., 2017. Delineation of enriched zones of Mo, Cu and Re by concentration-volume fractal model in Nowchun Mo-Cu porphyry deposit, SE Iran. Iranian Journal of Earth Sciences. 9(1), 64–72.

[24]. Mirzaei, M., Afzal, P., Adib, A., Rahimi, E., and Mohammadi, Gh., 2020. Detection of zones based on ore and gangue using fractal and multivariate analysis in Chah Gaz iron ore deposit, Central Iran. Journal of Mining and Environment. 11(2), 453-466. Doi: 10.22044/jme.2020.9111.1801.

[25]. Aliyari, F., Afzal, P., Lotfi, M., Shokri, S., and Feizi, H., 2020. Delineation of geochemical haloes using the developed zonality index model by multivariate and fractal analysis in the Cu–Mo porphyry deposits. Applied Geochemistry. 121, 104694. https://doi.org/10.1016/j.apgeochem.2020.104694.

[26]. Mark, D.M. and Aronson, P.B., 1984. Scale-Dependent Fractal Dimensions of Topographic Surfaces: An Empirical Investigation, with Applications in Geomorphology and Computer Mapping. Mathematical Geology, 16(7), 671-683. https://doi.org/10.1007/BF01033029.

[27]. Thorarinsson, F. and Magnusson, S.G., 1990, Bouguer density determination by fractal analysis: Geophysics, 55(7), 932-935. https://doi.org/10.1190/1.1442909.

[28]. Mehrnia, S.R., Ebrahimzadeh Ardestani, V., and Teymoorian, A., 2013. Application of fractal method to determine the Bouguer density of Charak Region (South of Iran). Iranian Journal of Geophysics, 7(1), 34-50 (in Persian).

[29]. Holland, H.D., 2005. Sedimentary Mineral Deposits and the Evolution of Earth's Near-Surface Environments. Society of Economic Geologists, Inc. Economic Geology, 100(8), 1489-1509. http://dx.doi.org/10.2113/gsecongeo.100.8.1489.

[30]. Haldar, S.K., 2017. Mineral Exploration Principles and Applications. Elsevier, 378 PP.

[31]. Russ, J.C., 1994. Fractal Surfaces. Springer Science & Business Media, Plenum Press, New York (313 pp.).

[32]. Agterberg, F.P., 2012. Multifractals and geostatistics. Journal of Geochemical Exploration. 122, 113-122. https://doi.org/10.1016/j.gexplo.2012.04.001.

[33]. Mehrnia, S.R., 2017. Application of Fractal Technique for Analysis of Geophysical- Geochemical Databases in Tekieh Pb-Zn Ore Deposit (SE of Arak). Journal of Economic Geology (ISSN 2008-7306). 8(2).

[34]. Mehrnia, R., 2013. Application of fractal geometry for recognizing the pattern of textural zoning in epithermal deposits (case study: Sheikh-Darabad Cu-Au indices, East-Azarbaijan province). Journal of Economic Geology (in Persian), 5(1), 23-36.

[35]. Pourfaraj, H., 2016. Structural analysis of fault systems in Mehdiabad Zn-Pb mine area, SE Yazd. [Unpublished MSc Thesis], Tarbiat Modares University, Iran, 192 pp.

[36]. G.S.I., 1988. Geological studies on the Mehdiabad Lead and Zinc Project (Unpubl. internal report).

[37]. Ankomah, A.B., 1992. Magnesium and pH Effect on Zinc Sorption by Goethite. Soil Science. 154(3), 206-213.

[38]. Reichert, J., Borg, G., and Rashidi, B., 2003. Mineralogy of calamine ore from the Mehdi Abad zinc-lead deposit, Central Iran. Conference 7th Biennial Meeting, Society for Geology Applied to Mineral Deposits; Mineral exploration and sustainable development, Athens. 97-102.

[39]. Ghasemi, M., 2006. Formation Mechanism of the Mehdiabad Zn–Pb Deposit and its Comparison with Other Near Lead and Zinc Deposits [Unpublished MSc Thesis], Research Institute of Earth Sciences, Geological Survey and Mineral Exploration of Iran, Iran, 238 pp.

[40]. Reichert, J., 2007. A Metallogenetic Model for Carbonate hosted Non-sulfide Zinc Deposits based on Observations of Mehdiabad and Iran Kouh, Central and Southwestern Iran [Unpublished PhD Thesis], University of Martin Luther, Shillong, 129 pp.

[41]. Ebrahim-Mohseni, M., 2011. Study of genesis of Mehdiabad deposit using fluid inclusion and stable isotope [Unpublished MSc Thesis], Damghan University, Damghan, Iran, 166 pp.

[42]. Maghfouri, S., 2017. Geology, Geochemistry, Ore Controlling Parameters and Genesis of Early Cretaceous Carbonate-clastic Hosted Zn-Pb Deposits in Southern Yazd Basin, with Emphasis on Mehdiabad Deposit [Unpublished PhD Thesis], Tabriz University, Iran, 475 PP.

[43]. Teymoorian-Motlagh, A., Ebrahimzadeh-Ardestani, V., and Mehrnia, R., 2012. Fractal method for determining the density of the stone tablet in Charak region (southern Iran). Life Science Journal. 9(4).

[44]. Bonham-Carter, G.F., 1994. Geographic Information Systems for Geoscientists: Modelling with GIS. Pergamon (402 pp).

[45]. Cheng, Q., 2006. Multifractal modelling and spectrum analysis: method and applications to gamma ray spectrometer data from southwestern Nova Scotia, Canada. Science China Earth Sciences. 49(3), 283-294. https://doi.org/10.1007/s11430-006-0283-y.

[46]. Tan, Q. and Xu, X., 2014. Comparative Analysis of Spatial Interpolation Methods: an Experimental Study. Sensors & Transducers Journal. 165(2), 155-163.

[47]. Xie, Sh., Cheng, Q., Ke, X., Bao, Zh., Wang, Ch., and Quan, H., 2008. Identification of Geochemical Anomaly by Multifractal Analysis. Journal of China University of Geosciences. 19(4), 334-342. https://doi.org/10.1016/S1002-0705(08)60066-7.

[48]. Morison, G., 2003. AMIRA Project, Revised version: Evaluating of Gold Mineralization Potentials in Queensland Epithermal Systems, Queensland J.C Univ. press, Queensland, Australia, 249 pp.

[49]. Akbari, E. and Mehrnia, R., 2013. Association of Silica Fractal Distribution with Gold Mineralization: a case study from the Takmeh-Dash Region, NW of Iran. Journal of Tethys. 1(4), 241-253.

[50]. Cheng, Q., 2007. Mapping singularities with stream sediment geochemical data for prediction of undiscovered mineral deposits in Gejiu, Yunnan Province, China. Ore Geology Reviews. 32(1-2), 314-324. https://doi.org/10.1016/j.oregeorev.2006.10.002.

[51]. Khaled, A., Cheng, Q., and Chen, Zh., 2007. Multifractal power spectrum and singularity analysis for modelling stream sediment geochemical distribution patterns to identify anomalies related to gold mineralization in Yunnan Province, South China. Geochemistry: Exploration, Environment, Analysis. 7(4), 293-301. https://doi.org/10.1144/1467-7873/06-116.

ارزیابی مدل فرکتالی پراش-مسافت در شناسایی بی‌هنجاری‌های ژئوشیمیایی کالامین مجتمع معدنی مهدی-آباد، ایران مرکزی

نسرین صدرمحمدی[1]*، سید رضا مهرنیا[2]، خلیل رضایی[1]، سلما کادی أغلو[3] و محمود هنرور[4]

۱- بخش زمین‌شناسی، دانشگاه خوارزمی، تهران، ایران

۲- بخش زمین‌شناسی، دانشگاه پیام‌نور، تهران، ایران

۳- بخش مهندسی ژئوفیزیک، دانشگاه آنکارا، ترکیه

۴- شرکت مهندسین مشاور زمین آب پی، تهران، ایران

چکیده:

در این مقاله، یک مدل‌سازی رابطه نمایی به نام مدل واریو- فرکتال به منظور درک تفاوت‌های بین توزیع خطی و غیرخطی عناصر و کاربرد آن برای اکتشاف مواد معدنی در کانسار معدنی کالامین روی-سرب معرفی شده است. از نظر فرضی، از آنجا که پهنه‌بندی ژئوشیمیایی عناصر فوق‌کانساری و تحت‌کانساری معیار اساسی برای ارزیابی پتانسـیل‌های کانی‌سازی پنهان/ اصلی اسـت، این فرضـیه را می‌توان با ترسـیم سـطوح فراکتال عناصـر به عنوان شـواهد هندسـی پهنه‌بندی اولیه ژئوشیمیایی عناصر موجود در معدن کالامین آزمایش کرد. مقایسه نتایج رگرسیون خطی با ضرایب توزیع پواسون، نشان دهنده تمایل نسبی عناصر به سمت توزیع غیرخطی است. بنابراین، برای ترسیم سطوح فراکتال عناصر به عنوان ویژگی‌های هندسی مربوط به توزیع‌های خود سازمان‌یافته مناسب، از یک معادله لگاریتمی به‌دسـت آمده از رابطه پراش-مسافت (نمایی) اسـتفاده می‌شـود. در این کار تحقیقاتی، بیان واریو-فراکتال پهنه‌بندی ژئوشـیمیایی دارای عناصـر کمیاب با توزیع غیرخطی اسـت. نتایج به دست آمده نشـان می‌دهد که سـطوح کسـری کالامین عمدتاً از انواع خودسـازمان‌یافته اسـت که ۳ >FD> ۲ به عنوان "سـطوح واقعی فراکتال" واقع شده است، اگرچه ۳ عنصر در جمعیت‌های شبه‌فراکتال به نام " سطوح نزدیک به سطح براونی" در اینجا پدیدار شده است. علاوه بر این، سطوح فراکتال کالامین می‌تواند در مناطق بی‌هنجاری گسترش یابد یا ممکن است به عنوان انواع محدودی از مدل نهایی توزیع شود، که یک الگوی مبتنی بر فراکتال از پهنه‌بندی ژئوشیمیایی عناصر برای ارزیابی پتانسیل کانی‌سازی هایپوژنیک است و ۶ منطقه هدف شامل ۱۰ عنصر با سطوح واقعی فراکتال و ۳ عنصر با سطوح نزدیک به سطح براونی توسط شواهد کانی‌شناسی تأیید و اولویت‌بندی شده است.

کلمات کلیدی: سطوح براونی، کالامین، کانی‌سازی، غیرسولفیدی، مدل‌سازی واریو-فرکتال.